Macromolecular Rapid Communications
www.mrc-journal.de

Microgel-Crosslinked Thermo-Responsive Hydrogel Actuators with High Mechanical Properties and Rapid Response

*Yanyu Yang, Ying Xiao, Xiang Wu, Junjie Deng, Rufang Wei, Ashuang Liu, Haiyang Chai, and Rong Wang**

Smart hydrogels responsive to external stimuli are promising for various applications such as soft robotics and smart devices. High mechanical strength and fast response rate are particularly important for the construction of hydrogel actuators. Herein, tough hydrogels with rapid response rates are synthesized using vinyl-functionalized poly(*N*-isopropylacrylamide) (PNIPAM) microgels as macro-crosslinkers and *N*-isopropylacrylamide as monomers. The compression strength of the obtained PNIPAM hydrogels is up to 7.13 MPa. The response rate of the microgel-crosslinked hydrogels is significantly enhanced compared with conventional chemically crosslinked PNIPAM hydrogels. The mechanical strength and response rate of hydrogels can be adjusted by varying the proportion of monomers and crosslinkers. The lower critical solution temperature (LCST) of the PNIPAM hydrogels could be tuned by copolymerizing with ionic monomer sodium methacrylate. Thermo-responsive bilayer hydrogels are fabricated using PINPAM hydrogels with different LCSTs via a layer-by-layer method. The thermo-responsive fast swelling and shrinking properties of the two layers endow the bilayer hydrogel with anisotropic structures and asymmetric response characteristics, allowing the hydrogel to respond rapidly. The bilayer hydrogels are fabricated into clamps to grab small objects and flowers that mimicked the closure of petals, and it shows great application prospects in the field of actuators.

1. Introduction

Stimuli-responsive hydrogels have attracted great research interest for their potential applications in soft robotics,[1] artificial muscle,[2] sensors,[3] and smart devices,[4] due to their ability to change dimension and other properties in response to environmental stimuli such as temperature,[5] ionic strength,[6] pH,[7] light,[8] and magnetism field.[9] The driving force of hydrogel actuators primarily arises from the expansion and/or contraction deformations.[10,11] Various hydrogel devices with heterogeneous structures and properties have been fabricated by precisely controlling the spatial distribution of the responsive domains in the hydrogel network.[12,13] However, the response rate of most responsive hydrogels through volume changes caused by water intake or loss is slow. In addition, conventional chemically crosslinked hydrogels are brittle and fragile because of the lack of energy dissipation mechanisms.[14] It remains a great challenge to fabricate strong and tough hydrogel devices with a rapid response speed for practical applications.

Poly(*N*-isopropylacrylamide) (PNIPAM) hydrogel is a typical temperature-sensitive hydrogel with a reversible volume phase transition at ≈32 °C,[15] making them ideal for fabrication of stimuli-responsive actuators. The phase transition temperature of PNIPAM hydrogel can be modulated by copolymerization with hydrophilic or hydrophobic units,[15] facilitating the hydrogel's responsiveness to a wide range of temperatures and thereby broadening its

Y. Yang, J. Deng, R. Wei, A. Liu, H. Chai, R. Wang
Cixi Biomedical Research Institute
Wenzhou Medical University
Zhejiang 315300, P. R. China
E-mail: rong.wang@nimte.ac.cn

Y. Yang, Y. Xiao, J. Deng, R. Wei, A. Liu, H. Chai, R. Wang
Zhejiang International Scientific and Technological Cooperative Base of Biomedical Materials and Technology
Institute of Biomedical Engineering
Ningbo Institute of Materials Technology and Engineering
Chinese Academy of Sciences
Ningbo 315201, P. R. China

Y. Yang, Y. Xiao, J. Deng, R. Wei, A. Liu, H. Chai, R. Wang
Ningbo Cixi Institute of Biomedical Engineering
Ningbo 315300, P. R. China

X. Wu
Ningbo Medical Center Li Huili Hospital
Health Science Center
Ningbo University
Ningbo 315000, P. R. China

The ORCID identification number(s) for the author(s) of this article can be found under https://doi.org/10.1002/marc.202300643

DOI: 10.1002/marc.202300643

potential applications in the field of actuators. However, the deswelling rate of conventional PNIPAM hydrogel is slow due to the formation of a collapsed polymer network and a dense skin layer after the ambient temperature increases above lower critical solution temperature (LCST), limiting the diffusion of water out of the hydrogel.[16] This drawback greatly constrains the applicability of thermo-responsive PNIPAM hydrogel devices. Strategies such as construction of comb-type architectures,[17] pore channels,[18] and nanocomposite structures[19] have been proposed to improve the response rate of PNIPAM hydrogels. On the other hand, tough PNIPAM hydrogels via strategies including composition of nanogels,[20] formation of interpenetrating polymer network,[21] double network,[22] and slide ring structure[23] have been developed. However, these approaches could compromise the stimulus sensitivity as well as the equilibrium swelling rate of the hydrogel.[24] It is still an issue of significant importance to simultaneously improve the mechanical strength and response speed of PNIPAM hydrogels.

For actuator applications, rapid response is essential to obtain instantaneous and significant feedback after exposure to environmental stimuli, while it is also crucial to withstand large deformations. Micro/nanogels containing nanocomposite structures have been proposed as a promising method that can simultaneously enhance the response rate and mechanical properties of hydrogels.[25] The structure, size, and functionality of micro/nanogels play an important role in the responsive rate of the hydrogel[26] by creating hydrophilic regions for channels to drain water out of the network during collapse.[27] In addition, micro/nanogels can be used as crosslinkers,[28] which can act as units for efficient energy dissipation, yielding enhanced mechanical properties in terms of strength and toughness.[29] Therefore, it is worthwhile to investigate the use of microgels as crosslinkers to simultaneously improve the responsiveness and mechanical properties of thermo-responsive hydrogels and soft actuators. Chu et al.[20] employed activated nanogels as crosslinkers to construct hydrogels with large responsive swelling ratio, rapid response rate, and high elasticity. Despite the successful enhancement in responsive rate and mechanical properties of the nanogel-crosslinked hydrogel, there still remains a challenge in precise control of the hydrogel's crosslinking structure due to the difficulty in controlling the concentration of residual vinyl groups in the nanogels during the one-step precipitation polymerization. In addition, application of the nanogel-crosslinked thermo-responsive hydrogels for the construction of bilayer actuators has not been explored.

In this work, vinyl-functionalized PNIPAM microgels were synthesized and used as crosslinking agents for fabrication of a novel PNIPAM-hydrogel with fast response rates and high mechanical properties. Unsaturated double bonds introduced via esterification reactions with hydroxyethyl methacrylate (HEMA) exhibit increased stability and can be precisely controlled. LCST of the PNIPAM hydrogel was adjusted by addition of hydrophilic monomer sodium methacrylate (SMA). The stimulus-response and mechanical properties of the hydrogel can be easily tuned by varying the contents of microgel crosslinkers and monomers. The response temperatures, swelling and deswelling rates, and mechanical strengths of the PNIPAM hydrogels were investigated. The PNIPAM hydrogels with different LCSTs were used to construct bilayer hydrogel devices. The bending behavior of the bilayer hydrogels was investigated with respect to varying hydrogel thickness ratios, ambient temperatures, and formulas. The thermo-responsive properties and potential applications of bilayer hydrogels as actuators and intelligent devices were explored.

2. Experimental Section

2.1. Materials

N-isopropylacrylamide (NIPAM, 99%), *N*,*N*′-methylenebis(2-propenamide) (MBAA, 95%), acrylic acid (AAc, >99%), potassium persulfate (KPS, AR, 99.5%), sodium dodecyl sulfate (SDS, ≥98.5%), hydroxyethyl methacrylate (HEMA, 96%), 1-[3-(dimethyl amino) propyl]−3-ethylcarbodiimide hydrochloride (EDC, 98%), 4-dimethylaminopyridine (DMAP, 99%), *N*,*N*,*N*′,*N*′-tetramethyl ethylenediamine (TEMED, 99%), sodium methacrylate (SMA, 99%), phenol red, and methylene blue (≥70%) were purchased from Aladdin Chemistry Co. Ltd. NIPAM was purified by recrystallization from hexane/acetone mixture and dried under vacuum. All other reagents were used as received.

2.2. Synthesis and Characterization of Vinyl-Functionalized Microgels

Vinyl-functionalized P(NIPAM-*co*-AAc) microgels were fabricated by precipitation polymerization and then esterification reaction. NIPAM and AAc were first copolymerized by free radical precipitation reaction to obtain P(NIPAM-*co*-AAc) microgels (denoted as MG). Briefly, 2.848 g NIPAM, 0.202 g AAc, and 0.064 g MBAA were dissolved in 200 mL of deionized water in a three-necked round-bottom flask fitted with a condenser. The mixture was degassed by nitrogen-bubbling for 15 min, followed by addition of 0.116 g SDS, and then it was heated to 70 °C. After 1 h, 4 mL of deionized water containing 0.16 g KPS was incrementally introduced to initiate the reaction, which continued for 4 h. The resultant microgels were subjected to dialysis using a dialysis bag (molecular weight cutoff: 8000–14 000 Da) against deionized water for at least 3 days.

Next, the P(NIPAM-*co*-AAc) microgels were esterified with HEMA to introduce vinyl groups. Briefly, 4.78 g EDC, 3.64 g HEMA, and 0.17 g DMAP were introduced into 100 mL of microgel dispersion, which contained ≈1.5 g MG. The mixture was subjected to continuous stirring at room temperature for 4 h. The solution was dialyzed using a cellulose dialysis bag (molecular weight cutoff: 8000–14 000 Da) against deionized water for at least 3 days. The products (denoted as MGV) were lyophilized and stored at −20 °C for further use.

^{1}H nuclear magnetic resonance (^{1}H NMR) spectra of the microgels were recorded on a Nuclear Magnetic Resonance (NMR, AVANCE NEO 400 MHz, Bruker, Germany) at room temperature using deuterated water as solvent. Fourier-transform infrared spectroscopy (FT-IR, IS 50, Thermo Fisher Scientific, United States) was employed to investigate the functional groups of the microgels before and after modification. The spectrum was recorded from 4000 to 400 cm^{-1} for lyophilized microgels in KBr pellets for 32 scans at the resolution of 4 cm^{-1}. The morphology of the microgels was observed using Transmission Electron Mi-

Table 1. Formulations for preparation of MGV-crosslinked PNIPAM hydrogels ($N_{100}M_x$ and $N_{100-y}S_yM_x$) and chemical crosslinked PNIPAM hydrogel (NG).

Hydrogel	NIPAM [g]	SMA [g]	MGV [g]	MBAA [mg]	KPS [mg]	TEMED [μL]	H_2O [mL]
$N_{100}M_1$	1.694	0	0.1	0	4.2	20	10
$N_{100}M_2$	1.694	0	0.2	0	4.2	20	10
$N_{100}M_3$	1.694	0	0.3	0	4.2	20	10
$N_{100}M_4$	1.694	0	0.4	0	4.2	20	10
$N_{99}S_1M_3$	1.678	0.016	0.3	0	4.2	20	10
$N_{95}S_5M_3$	1.644	0.049	0.3	0	4.2	20	10
$N_{97}S_3M_3$	1.525	0.162	0.3	0	4.2	20	10
NG	1.694	0	0	2.3	4.2	20	10

croscopy (TEM, HT7800, Hitachi, Japan), and the diameter of the microgels was measured using ImageJ (Version 1.53k).

2.3. Preparation of Monolayer Hydrogels

A specified amount of NIPAM and SMA monomers (the total concentration was fixed at 1.5 mol L^{-1}), MGV, and KPS were added into 10 mL of deionized water in an ice bath and stirred for 2 h. TEMED was then added to the mixture under stirring, and the resulting dispersion was promptly injected into a mold consisting of two glass plates sandwiching a silicone gasket with 2 or 5 mm in thickness. The precursor dispersion was incubated at room temperature for 48 h to obtain bulk hydrogels. The PNIPAM and P(NIPAM-*co*-SMA) hydrogels crosslinked by microgels were denoted as $N_{100}M_x$ and $N_{100-y}S_yM_x$, where x and y represent the concentration of microgels (in weight percentage) and SMA monomers (in molar percentage), respectively. For comparison, chemically crosslinked PNIPAM hydrogel (denoted as NG hydrogel) was prepared in a similar manner as described above, with MBAA instead of MGV microgels used as the crosslinker. The formulation for the hydrogel preparation is given in **Table 1**.

2.4. Preparation of Bilayer Hydrogels

The bilayer hydrogels were fabricated in a two-step process. First, single layer $N_{100-y}S_yM_3$ hydrogel was prepared using a glass mold sandwiching a silicone gasket with various thicknesses (0.5, 1.0, or 1.5 mm) as described above, but the reaction time was reduced to 20 min. Methylene blue at 0.1 mg mL^{-1} was added in the $N_{100-y}S_yM_3$ prepolymer solution for visualization of the hydrogel layer. After that, the as-obtained partially formed $N_{100-y}S_yM_3$ hydrogel was placed in a new silicone gasket with a thickness of 2 mm. A precursor solution of $N_{100}M_3$ was injected into the mold on the top of the $N_{100-y}S_yM_3$ layer. In addition, phenol red was added in the $N_{100}M_3$ precursor solution at a concentration of 0.1 mg mL^{-1}, for visualization of the $N_{100}M_3$ layer. The precursor solution was incubated at room temperature for 48 h to obtain a bilayer hydrogel. The bilayer hydrogel was swollen in deionized water for 30 min, freeze-dried, and frozen fractured in liquid nitrogen to obtain the cross-section, the fractured surface was sputtered with gold, and the interface morphology of the bilayer hydrogels was observed using a field emission scanning electron microscope (FE-SEM, Hitachi, Regulus 8283, Japan).

2.5. Mechanical Measurement

For compression testing, cylindrical samples (9 mm in diameter and 5 mm in thickness) were tested using a universal testing machine (CMT-1104, China) at a strain rate of 10% per minute until 98% strain. The modulus of elasticity was calculated as the slope of the stress-strain curve for strains ranging from 0 to 10%. At least five parallel samples were tested for compression. Toughness of the hydrogel was defined by the area under the compressive stress-strain curve. In the cyclic compression experiment, the hydrogel sample underwent repeatedly loading to 80% strain and unloading for 5 consecutive cycles. The energy dissipated in each cycle is quantified by the area enclosed within the loading-unloading curve loop. In the tensile tests, strip specimens (2 mm × 1 mm) with a gauge length of 14 mm were stretched at a crosshead speed of 50 mm min^{-1}. The modulus is calculated based on the strain range of 0% to 10%.

2.6. Determination of LCST of Hydrogels

The LCST of hydrogels was determined by Differential Scanning Calorimetry (DSC, Discovery 2500, TA, United States). DSC thermograms of the samples were taken at the heating rate of 2 °C min^{-1}. LCST of the hydrogel samples was determined from the peaks in the DSC curve.[30]

2.7. Analyze of Swelling/Deswelling Properties of Hydrogels

For the swelling test, hydrogels (9 mm in diameter and 2 mm in thickness) were soaked in 10 mL of deionized water at 25 °C for 24 h to reach equilibrium. The swelling ratio of each sample was calculated by the following Equation (1):

$$\text{Swelling Ratio} = \frac{w_t - w_0}{w_0} \times 100\% \quad (1)$$

where W_0 and W_t are the weights (g) of the hydrogel samples before and after swelling, respectively.

To investigate the thermo-responsive deswelling behavior of the hydrogels with different contents of microgel crosslinker, the hydrogels (9 mm in diameter and 2 mm in thickness) were first swell equilibrium at 25 °C, and then quickly transferred to a water bath preheated to 40 °C. A digital camera was used to record the shrinkage behavior of the hydrogel. The dimensions of the hydrogel were measured using digital pictures taken from the recorded video. The deswelling ratio was defined as Equation (2):

$$\text{Deswelling Ratio} = \frac{d_0 - d_t}{d_0} \times 100\% \quad (2)$$

where d_t and d_0 are the diameters of the hydrogel sample at time t and the beginning (t = 0, equilibrated in 25 °C water), respectively.

2.8. Small-Angle X-ray Scattering

SAXS measurements were carried out on a Xenocs GeniX 3D Cu ULD micro-beam X-ray generator. The wavelength of X ray radiation was 0.154 nm. 2D SAXS patterns were collected by using a MAR345 X-ray detector (marXperts, Norderstedt, Germany) with a resolution of 2048 × 2048 pixels. The sample to detector distance was 3000 mm. The SAXS image acquisition time of each data frame was set as 300 s.

2.9. Thermo-Responsive Bending Behavior of Hydrogels

To investigate the thermo-responsive behavior of single layer hydrogel, $N_{100}M_3$ and $N_{100-y}S_yM_3$ hydrogels (9 mm in diameter and 2 mm in thickness) as synthesized were directly immersed in deionized water at temperatures of 30, 40, or 50 °C without swelling. The changes in the diameter of the hydrogels were recorded using a camera and measured using a protractor.

To investigate the thermo-responsive bending behavior of bilayer hydrogels, the bilayer hydrogel with a total thickness of 2 mm containing an $N_{100-y}S_yM_3$ layer and an $N_{100}M_3$ layer (ratio of thickness: 1:3, 1:1, 3:1) was prepared. The bilayer sample was cut into strips of 25 mm × 5 mm, and then immersed individually in deionized water preheated to a determined temperature. For investigation of the recovery properties of the bilayer hydrogel, it was consecutively immersed in water baths of 40 and 20 °C. The stimuli-responsive behavior was recorded using a digital camera. The bending angle of the bilayer hydrogel in the digital image was measured, and the curve of bending angle versus time was plotted.

2.10. Bilayer Hydrogel Actuator Demonstration

Bilayer hydrogel (thickness ratio of $N_{97}S_3M_3$ to $N_{100}M_3$: 1:1) was cut into a strip of 25 mm × 5 mm. It was fastened using a metal wire, and immersed in a water bath at 40 °C. The process of the bilayer hydrogel gripper grasping a plastic plate was recorded using a digital camera. Bilayer hydrogels (thickness ratio of $N_{97}S_3M_3$ to $N_{100}M_3$: 1:1) were cut into petal shapes using a mold, and fixed to a plate to fabricate artificial flowers. It was then immersed in a water bath at 40 °C. The transformation of the artificial flower was recorded using a digital camera.

3. Results and Discussion

3.1. Preparation and Characterization of Vinyl-Functionalized Microgels

Vinyl-functionalized P(NIPAM-*co*-AAc) microgels were synthesized via a two-step process according to the previous literature.[31] First, P(NIPAM-*co*-AAc) microgels (MG) were fabricated by precipitation polymerization of NIPAM and AAc as monomer and MBAA as crosslinker in the presence of surfactant SDS. Vinyl-functionalized microgel (MGV) was then obtained by esterifying the carboxyl groups on the P(NIPAM-*co*-AAc) microgel and the hydroxyl groups on HEMA (**Figure 1**).

P(NIPAM-*co*-AAc) microgels before and after grafting of vinyl groups were characterized using ^{1}H NMR (**Figure 2a**). Successful introduction of vinyl groups on P(NIPAM-*co*-AAc) microgel was confirmed by the appearance of new peaks at 6.07 and 5.70 ppm in the ^{1}H NMR spectrum. The new peak at 4.21 ppm (protons in -O-CH_2-CH_2-O-) further confirmed the successful coupling of HEMA with the microgels. From the ratio of the integration area of the peak of protons in the vinyl groups and the peak of protons in $CH(CH_3)_2$ in NIPAM (3.84 ppm), it is estimated that ≈16% of carboxyl groups in the microgel reacted with HEMA. The FT-IR spectrum results (Figure 2b) also confirmed that part of the carboxyl groups on MG microgels reacted with HEMA, causing a red shift of the carbonyl stretching band (from 1720 cm^{-1} in MG to 1702 cm^{-1} in MGV). The diameter of the MG microgel observed using TEM was ≈295 ± 18 nm (Figure 2c), whereas that of MGV after vinyl functionalization was about 188 ± 28 nm. It is likely that grafting HEMA chains onto the MG microgels consumed some hydrophilic carboxyl groups, and increased the hydrophobicity of the microgel cores, thereby resulting in the shrinkage of the network.[32]

3.2. Preparation and Mechanical Properties of Microgel-Crosslinked $N_{100}M_x$ Hydrogels

The obtained vinyl-functionalized P(NIPAM-*co*-AAc) microgels were used as macro-crosslinkers to synthesize bulk hydrogels with NIPAM as monomers by free radical polymerization (Figure 1). PNIPAM hydrogel chemically crosslinked by MBAA was prepared for comparison. The mechanical strength of the hydrogels was first investigated. In **Figure 3a** and Movie S1, Supporting Information, NG samples exhibit brittleness, rendering them unable to withstand compression, whereas $N_{100}M_3$ demonstrates outstanding elastic properties. Figure 3b shows typical compressive stress-strain curves of NG hydrogel and $N_{100}M_x$ hydrogels crosslinked by different contents of microgels. As can be seen, the chemically crosslinked NG hydrogels were brittle with a compressive strength of 0.11 MPa and a compressive modulus of 4.54 MPa. As the MGV content increased from 1% to 3%, the compressive strength of the hydrogel increased from 1.32 MPa of $N_{100}M_1$ to 7.13 MPa of $N_{100}M_3$. When the MGV content was further increased to 4%, the compressive strength of the $N_{100}M_4$ hydrogel decreased to 2.94 MPa. The modulus of the $N_{100}M_x$ hydrogel first decreased to 2.50 MPa when 1% of MGV was added, and then increased continuously to 5.51 MPa when the MGV content increased to 4% (Figure 3c). The toughness increased from about 0.05 MJ m^{-3} of $N_{100}M_1$ to 0.37 MJ m^{-3} of $N_{100}M_3$,

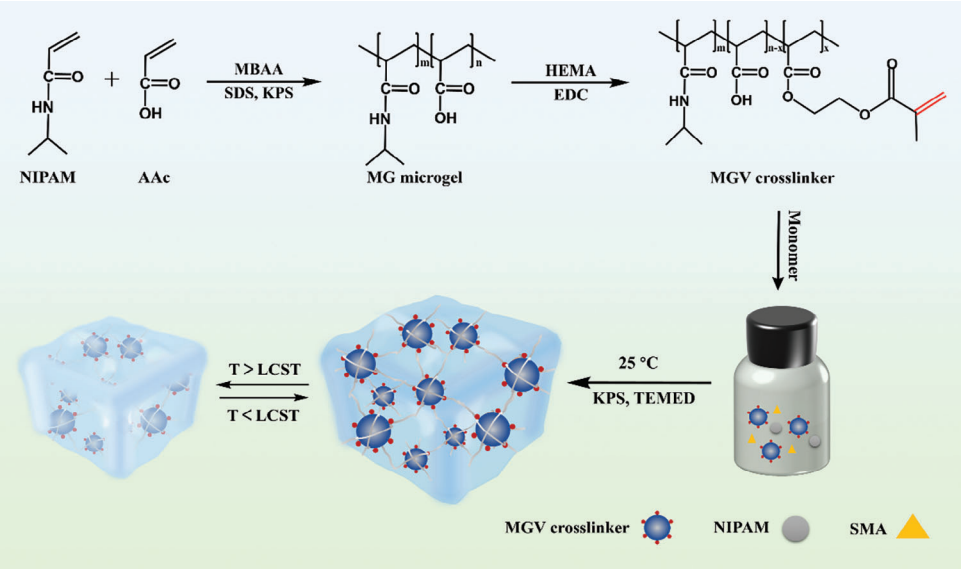

Figure 1. Preparation process of P(NIPAM-*co*-AAc) (MG), vinyl-functionalized microgel (MGV) and MGV microgel-crosslinked PNIPAM hydrogel with thermo-responsive property.

and then decreased to 0.14 MJ m^{-3} of $N_{100}M_4$ (Figure 3d). As shown in Figure S1, Supporting Information, cyclic compression testing of $N_{100}M_x$ hydrogel showcased remarkable fatigue resistance throughout five cycles of loading-unloading, spanning from 0% to 80%. The loading-unloading curves for different cycles almost overlapped, suggesting an immediate recovery of the hydrogel due to the energy dissipation mechanism. The $N_{100}M_3$ hydrogel exhibits optimal energy dissipation, reaching ≈0.37 MJ m^{-3}. This exceptional fatigue resistance is credited to the microgels functioning as macroscopic crosslinkers, deforming to efficiently dissipate energy during compressive loading. It can be clearly observed from Figure S2, Supporting Information, that when the $N_{100}M_3$ hydrogel was not subjected to any compression, the SAXS scattering pattern was symmetrical and circular. However, when the $N_{100}M_3$ hydrogel was compressed by 90%, the microgeometry of the microgel undergoes deformation along the compression direction, indicating dissipation of energy. This exceptional fatigue resistance is credited to the microgels functioning as macroscopic crosslinkers, deforming to efficiently dissipate energy during compressive loading. As can be seen from the SEM images (Figure S3, Supporting Information), compared with the freeze-dried NG hydrogel (swollen overnight), the $N_{100}M_x$ hydrogel exhibits a higher porosity in the structure, and the porosity decreases with increase in the MGV crosslinkers.

These results indicated that the mechanical properties of the PNIPAM hydrogels could be improved by introduction of appropriate contents of P(NIPAM-*co*-AAc) microgel crosslinkers. In contrast to being crosslinked by chemical crosslinker MBAA, it has been reported that the macro-crosslinker could react in two different processes during polymerization. It created intercrosslinking structures between the polymer chains to improve the hydrogel toughness, and intra-crosslinking inside the macrocrosslinker to enhance the overall strength of the hydrogel.[33] This distribution offers advantages in terms of energy dissipation and crack passivation. On the one hand, the microgels crosslinked with the hydrogel network would be deformed reversibly by external forces to dissipate the energy and maintain the integrity of the hydrogel. On the other hand, the microgels would swell in the aqueous precursor solution and thus, allowing the monomers to diffuse into the microgel and form an interpenetrating network structure upon the formation of the hydrogel, resulting in a secondary mechanism of energy dissipation. However, when the microgel content becomes too high, an excess of crosslinking points in the system might hinder polymer chain elongation during polymerization, thereby reducing the mechanical performance of the hydrogel.[34] Excessive crosslinking agent impedes the elongation of molecular chains, while insufficient crosslinking agent diminishes the network structure. Hence, an appropriate content of crosslinker is important for superior energy dissipation of the hydrogel.

The NG hydrogel's brittleness precludes it from undergoing tensile testing, but the tensile properties of the $N_{100}M_X$ hydrogel show significant improvement compared to the NG hydrogel (Figure S4, Supporting Information). The tensile strengths of $N_{100}M_1$, $N_{100}M_2$, $N_{100}M_3$, and $N_{100}M_4$ hydrogels were 26.51, 24.88, 24.59, and 22.10 kPa, respectively. Additionally, the modulus experiences an increase from 5.18 kPa of $N_{100}M_1$ to 14.06 kPa of $N_{100}M_4$. The increased tensile strength in these hydrogels can be attributed to the presence of macro-crosslinkers in the microgels, which deform and effectively dissipate energy during the stretching process of the polymer chains.

3.3. LCST and Thermo-Responsive Behavior of $N_{100}M_x$ Hydrogels

Thermo-responsive hydrogels exhibit phase transition upon change of environment temperature, which is expressed as the LCST of the hydrogel. When the temperature exceeds the LCST of the hydrogel, its internal network structure collapses, causing a transition from transparency to a milky-white appearance,

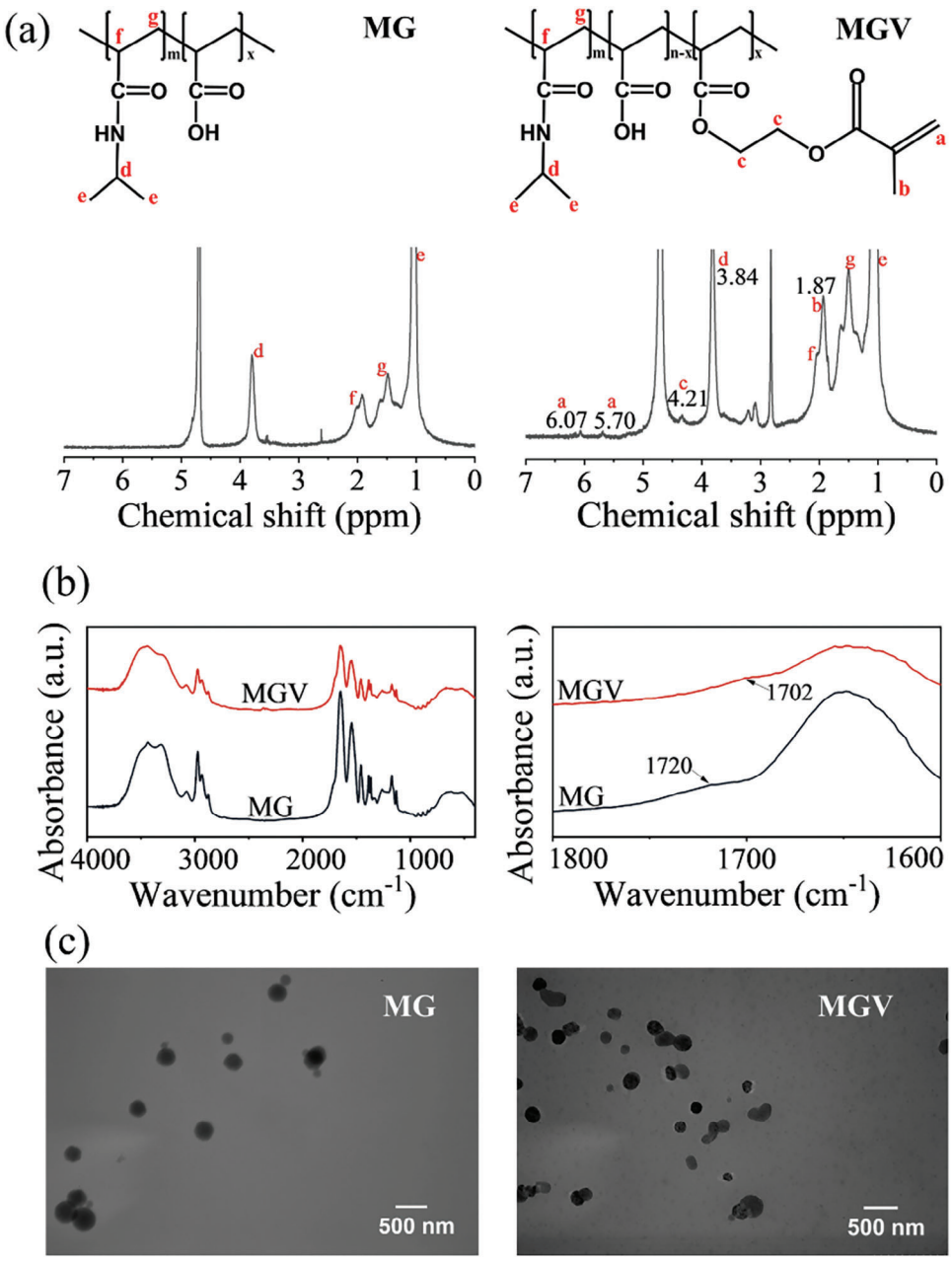

Figure 2. a) ^{1}H NMR spectra, b) FT-IR spectra, and c) TEM images of MG and MGV microgels.

accompanied by a reduction in volume. In this study, DSC was used to determine the LCST of PNIPAM hydrogels that were crosslinked by various MGV contents. The LCST of MBAA-crosslinked PNIPAM hydrogel was determined to be 32.0 °C (Figure 3e), which is in agreement with the previous study.[35] With addition of MGV microgel, the LCST of the hydrogel increased slightly to 34.4, 34.7, 35.0, and 35.6 °C, for $N_{100}M_1$, $N_{100}M_2$, $N_{100}M_3$, and $N_{100}M_4$ hydrogels, respectively. This could be attributed to that the presence of hydrophilic carboxyl groups in the MGV crosslinkers promotes the formation of hydrogen bonding with water, thus leading to an increase in the LCST of the hydrogels.[36]

At temperatures below the LCST, the PNIPAM hydrogels remain expanded. The crosslinking density of the hydrogel network affects its swelling properties.[37] As shown in Figure 3f, at temperatures below LCST (i.e., 25 °C), when the MGV content increased from 1% to 4%, the equilibrium swelling ratio of the hydrogels decreased from 452% to 250%, which was higher than that of the NG hydrogel (176%) under the same condition. This could be attributed to that the introduction of microgels significantly increased the swelling capacity of PNIPAM hydrogels by providing additional hydrophilic reservoirs in the PNIPAM matrix.[38] However, a high degree of crosslinking prevented hydrogel expansion and limited water penetration in the hydrogel

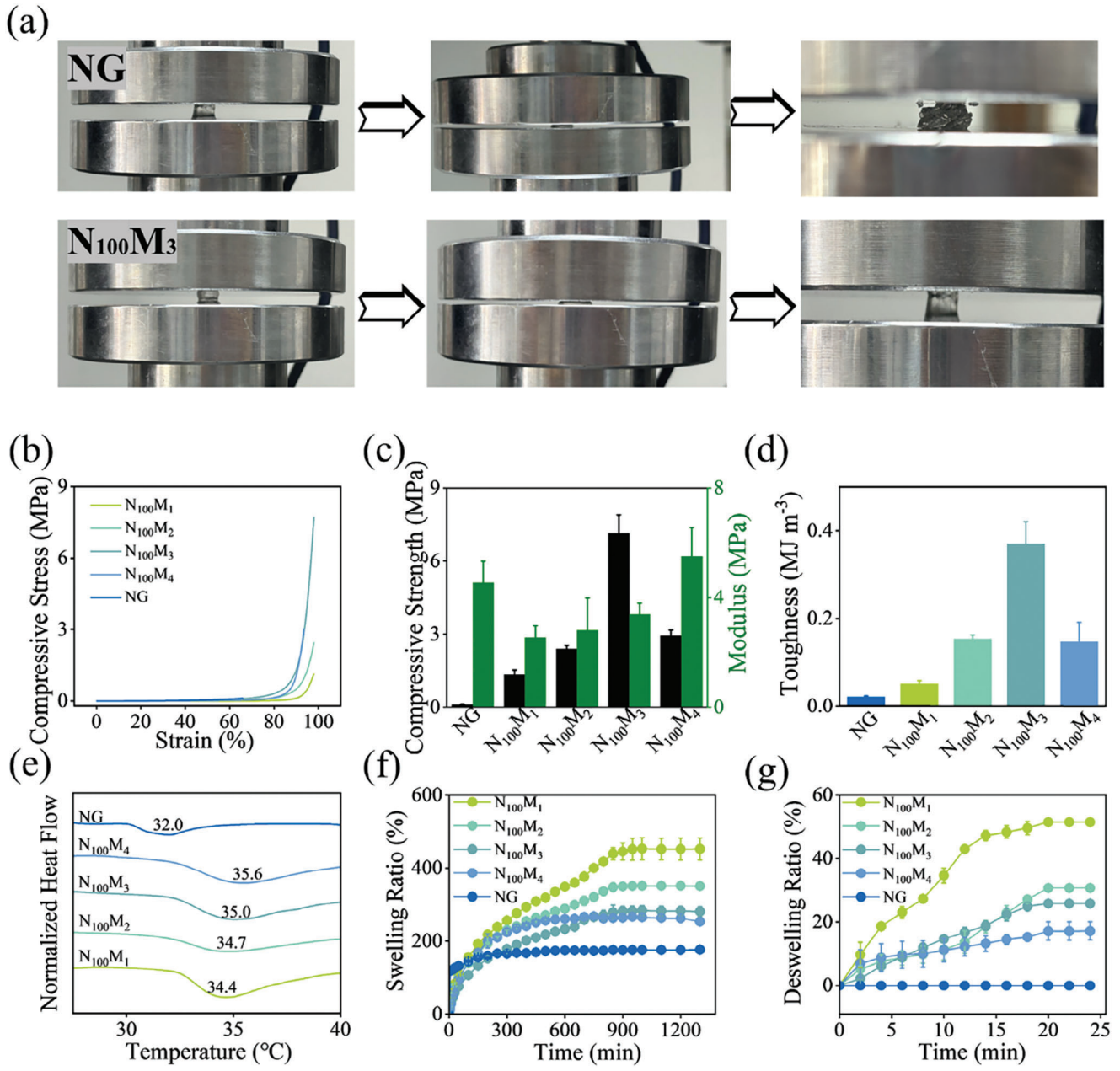

Figure 3. a) Digital photos showing NG and $N_{100}M_3$ hydrogels subjecting to 98% compression and then unloaded. b) Representative compressive stress-strain curves, c) compressive strength and modulus, d) toughness, e) DSC thermograms, f) swelling properties (incubated at 25 °C), and g) deswelling properties (incubated at 40 °C) of NG and $N_{100}M_x$ hydrogels.

network, thereby reducing the swelling property of the $N_{100}M_x$ hydrogels.

Hydrogels equilibrated at 25 °C were then immersed in a water bath preheated to 40 °C (T > LCST) to study their deswelling behavior. As shown in Figure 3g, all of the $N_{100}M_x$ hydrogels were deswelled at the evaluated temperature and reached a plateau after ≈20 min. With an increase in MGV content, the extent of the shrinkage of $N_{100}M_x$ hydrogels apparently reduced, from 51.5% of $N_{100}M_1$ to 17.1% of $N_{100}M_4$. A higher MGV content leads to the formation of a more rigid hydrogel structure, thereby constraining the mobility of polymer chains within the hydrogel.[39] This constraint supersedes the volume phase change performance of the PNIPAM chains in the network above LCST, leading to a reduced degree of shrinkage in $N_{100}M_4$ compared to $N_{100}M_1$. It is worth noting that the chemically crosslinked NG hydrogel showed almost no shrinkage, probably due to the dense skin layer limiting the diffusion of water molecules out of the hydrogel as reported previously.[16] In contrast, with MGV as the crosslinker, the flexible linear PNIPAM bridges between the microgels have low crosslinking constraints and high flexibility.[40] At temperatures higher than LCST, the small microgel responds fast and shrinks with the flexible linear PNIPAM chains, leading to the

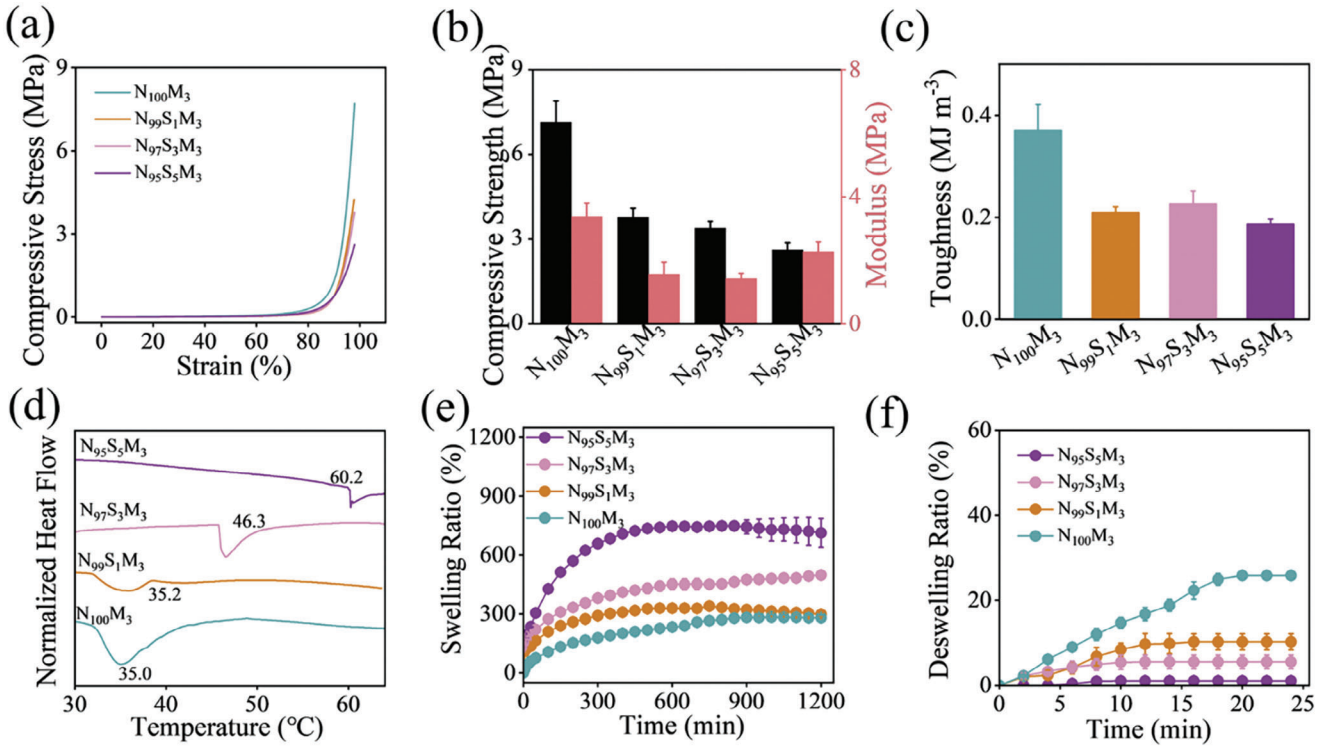

Figure 4. a) Representative compressive stress-strain curves, b) compressive strength and modulus, c) toughness, d) DSC thermograms, e) swelling properties (incubated at 25 °C), and f) deswelling properties (incubated at 40 °C) of $N_{100-y}S_yM_x$ and $N_{100}M_3$ hydrogels.

formation of interconnected microporous channels that allow the water molecules to escape.[41]

3.4. Preparation and Mechanical Properties of Microgel-Crosslinked $N_{100-y}S_yM_x$ Hydrogels

It is well established that copolymerizing hydrophilic units like SMA into the gels can augment the hydrophilicity of the network and elevate the equilibrium swelling ratio.[42,43] Given the superior mechanical properties of $N_{100}M_3$ hydrogels, it was chosen to copolymerize with SMA to adjust the mechanical properties, LCST, and swelling and deswelling capabilities of the hydrogels. Typical compressive stress-strain curves of the $N_{100-y}S_yM_3$ hydrogels were shown in **Figure** 4a. After incorporation of SMA units, the compressive strength decreased from 7.13 MPa of $N_{100}M_3$ to 3.78 MPa of $N_{99}S_1M_3$ hydrogel and 2.63 MPa of $N_{95}S_5M_3$ hydrogel. The modulus first decreased from 3.38 MPa of $N_{100}M_3$ to 1.56 MPa of $N_{99}S_1M_3$, and then increased from to 2.27 MPa of $N_{95}S_5M_3$, and the toughness decreased to about 0.2 MJ m^{-3} for all of the $N_{100-y}S_yM_3$ hydrogels. With the addition of the ionic SMA unit, the compressive strength, modulus, and toughness of $N_{100-y}S_yM_3$ hydrogels all decreased compared to those of $N_{100}M_3$ hydrogel (Figure 4b,c). The cyclic compression test of $N_{100-y}S_yM_x$ hydrogel also exhibited exceptional fatigue resistance over five loading-unloading cycles spanning from 0% to 80% (Figure S5, Supporting Information). The energy dissipation diminishes with the increasing SMA content. On the one hand, it was likely due to the increase in osmotic pressure and the reduction in the number of chain entanglements caused by the electrostatic repulsion of the ionic SMA units.[44] On the other hand, a reduction in NIPAM content might affect the hydrogen bonding between polymer chains. The microstructure of lyophilized $N_{100}M_3$ hydrogel (swollen overnight) is significantly different from that of lyophilized $N_{100-y}S_yM_3$ hydrogel (swollen overnight) (Figure S3, Supporting Information). The internal pore size of $N_{100-y}S_yM_3$ hydrogel gradually increases with the content of SMA.

Compared with $N_{100}M_3$ hydrogel, the stretchability of $N_{100-y}S_yM_x$ hydrogel increased with increasing SMA content (Figure S6, Supporting Information). The tensile strength of hydrogels was 20.53 kPa for $N_{99}S_1M_3$, 24.67 kPa for $N_{97}S_3M_3$, and 32.33 kPa for $N_{95}S_5M_3$. In addition, the tensile modulus was determined to 11.82, 10.26, and 13.47 kPa for $N_{99}S_1M_3$, $N_{97}S_3M_3$, and $N_{95}S_5M_3$, respectively. The slight enhancement in tensile strength can be attributed to ionic interactions between SMA repeating units.[45]

3.5. LCST and Thermo-Responsive Behavior of $N_{100-y}S_yM_x$ Hydrogels

The LCST of the hydrogel was also adjusted by changing the SMA ratio. As shown in Figure 4d, the LCST of $N_{99}S_1M_3$, $N_{97}S_3M_3$, and $N_{95}S_5M_3$ hydrogels was 35.2, 46.3, and 60.2 °C, respectively, which was higher than that of $N_{100}M_3$ hydrogel (35.0 °C). It can be considered that the incorporation of SMA increased the hydrophilicity of the hydrogel, resulting in a high hydration effect

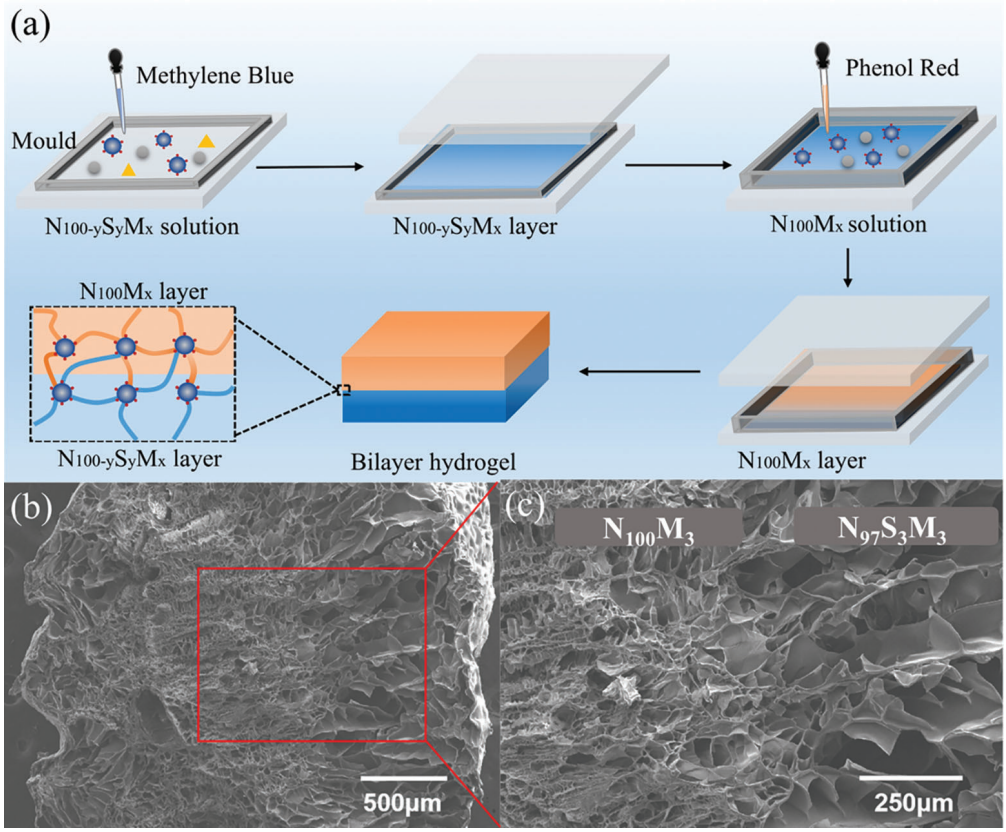

Figure 5. a) Schematic illustration of the preparation process of bilayer hydrogel. b,c) SEM images of the cross-section of an $N_{97}S_3M_3$-$N_{100}M_3$ bilayer hydrogel.

of the hydrogel, thus increasing the temperature of phase transition of the hydrogels.

The swelling behavior of the $N_{100-y}S_yM_3$ hydrogels was plotted in Figure 4e. As the content of the hydrophilic SMA units increased, the swelling rate increased from 280% of $N_{99}S_1M_3$ to 713% of $N_{95}S_5M_3$. This is because the introduction of hydrophilic SMA units increased the hydrophilicity and swelling degree of the hydrogel.[46] Similarly, the deswelling behavior of $N_{100-y}S_yM_3$ hydrogel was observed by transferring an equilibrated hydrogel to a water bath with an elevated temperature (40 °C). As shown in Figure 4f, $N_{95}S_5M_3$ and $N_{97}S_3M_3$ hydrogels showed minimal changes over 20 min, since the temperature was below their LCST (46.3 and 60.2 °C, respectively, Figure 4d). The $N_{99}S_1M_3$ hydrogel shrunk by 10.0% due to that the environment temperature exceeded the LCST of the $N_{99}S_1M_3$ hydrogel (35.2 °C).

3.6. Preparation and Morphology of Bilayer Hydrogels

Asymmetric responsiveness and anisotropic structure are essential factors in constructing effective thermo-responsive actuators with fast shape deformation upon temperature stimulation. In addition, reliable mechanical properties are critical to ensure their practical application. Based on the results above, $N_{100}M_3$ with superior mechanical properties was chosen as one layer, and $N_{97}S_3M_3$ was selected as the other layer, forming a dual-layer hydrogel actuator. These two hydrogel layers exhibited distinct LCSTs of 35.0 and 46.3 °C, respectively. The hydrogels also displayed varying swelling and deswelling characteristics, allowing the assembled bilayer hydrogel to possess rapid and obvious shape-changing behavior upon temperature stimulation. The bilayer hydrogel was prepared by a layer-by-layer polymerization method (**Figure 5a**). A partially polymerized $N_{97}S_3M_3$ hydrogel layer was first prepared, and then the $N_{100}M_3$ precursor for the second hydrogel layer was added to form an $N_{97}S_3M_3$-$N_{100}M_3$ bilayer hydrogel. Since the first $N_{97}S_3M_3$ layer was partially polymerized, the monomers in the $N_{100}M_3$ precursor could penetrate into the first layer. After polymerization, the polymer chains of the two layers at the interface were entangled. The interpenetration and entanglement of the PNIPAM chains and microgels ensured that the two hydrogel layers were tightly bonded, and no delamination was found (Figure 5b,c). Large pores with diameters of 60–80 μm were observed in the cross-section of the $N_{97}S_3M_3$ hydrogel, while a dense structure with a small pore size was found in the $N_{100}M_3$ hydrogel.

3.7. Thermo-Responsive Properties of Bilayer Hydrogels

Thermo-responsive behavior of the as-prepared bilayer hydrogel was investigated by measuring the bending angle change of the hydrogel after incubation in a water bath at a determined temperature (**Figure 6a**). For convenience, bilayer hydrogels were first prepared with equal thickness (i.e., 1 mm for each layer). It

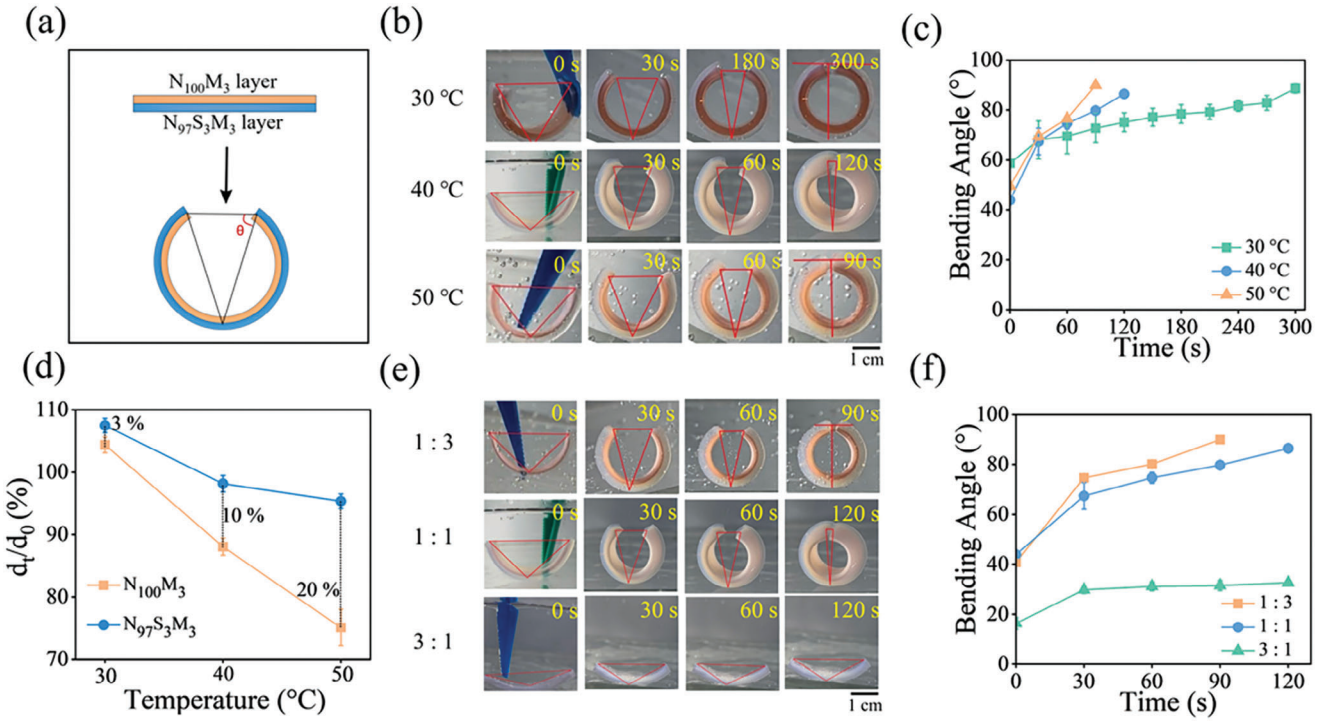

Figure 6. a) Schematic diagram of thermo-responsive behavior of the bilayer hydrogel strips, θ is defined as the bending angle of the bilayer hydrogel. b) Digital photos and c) bending angle of bilayer hydrogels in response to different temperatures. The thickness ratio of $N_{97}S_3M_3$ layer to $N_{100}M_3$ layer is 1:1. d) Thermal response behavior of a single-layer hydrogel at different temperatures, where d_0 and d_t represent the diameter of the single-layer hydrogel initially (i.e., 9 mm) and after 5 min of incubation, respectively. e) Digital photos and f) bending angles of bilayer hydrogels with different thickness ratios incubated at 40 °C. Scale bar is 1 cm.

was observed that the bilayer hydrogel bent toward the $N_{100}M_3$ layer at all the temperatures investigated (i.e., 30, 40, and 50 °C), either above or below the LCST of the hydrogels. As shown in Figure 6b,c, the time required for the bilayer hydrogel to achieve a 90° bend from its initial state (58.7° at 30 °C, 43.9° at 40 °C, 49.6° at 50 °C) was ≈300, 120, and 90 s, respectively. The higher the temperature was, the faster the bilayer hydrogel bent. Figure S7a, Supporting Information displayed that the bending rates of $N_{97}S_3M_3$-$N_{100}M_3$ bilayer hydrogel in pre-heated deionized water were 0.09° s^{-1} at 30 °C, 0.34° s^{-1} at 40 °C, and 0.45° s^{-1} at 50 °C, respectively. With an increase in temperature, the bending rate of the bilayer hydrogel progressively enhanced. The mechanism for the bending behavior of the hydrogel at different temperatures might be different. As noted in Figures 3d and 4d, the LCST of $N_{100}M_3$ and $N_{97}S_3M_3$ hydrogels was 35.0 and 46.3 °C, respectively. At 30 °C, the environmental temperature was lower than the LCSTs of both hydrogels, and the as-prepared $N_{100}M_3$ and $N_{97}S_3M_3$ hydrogels swelled at a d_t/d_0 ratio of 104% and 107%, respectively (Figure 6d). Due to the relatively higher swelling ratio of the $N_{97}S_3M_3$ layer, the bilayer bent toward the $N_{100}M_3$ side. At 40 °C, the temperature was higher than the LCST of $N_{100}M_3$ hydrogel, but lower than that of $N_{97}S_3M_3$. The $N_{97}S_3M_3$ hydrogel exhibited only a slight shrinkage, while the $N_{100}M_3$ hydrogel shrunk to a large d_t/d_0 ratio of 88%, leading to the bending of the bilayer hydrogel toward the $N_{100}M_3$ side. At 50 °C, which was higher than the LCST of both hydrogels, both of the two hydrogels shrunk quickly, reaching a d_t/d_0 ratio of 75% for $N_{100}M_3$ and 95% for $N_{97}S_3M_3$, respectively, causing the bilayer to bend quickly toward the $N_{100}M_3$ side. It is noteworthy that at 50 °C, the degree of shrinkage of the $N_{100}M_3$ layer was markedly higher than that of the $N_{97}S_3M_3$, and destruction of the bilayer structure was observed. Therefore, a relatively mild temperature of 40 °C was chosen for investigation of the thermo-responsive behavior of the bilayer hydrogel in the rest of the study.

The thermo-responsive behavior of the hydrogel actuator with different thickness ratios of the two layers was then studied (Figure 6e,f). As can be seen, the hydrogel actuator with a layer thickness ratio of 1:3 (i.e., 0.5 mm for $N_{97}S_3M_3$ and 1.5 mm for $N_{100}M_3$) achieved maximum bending angle from 40° to 90° in 90 s. The bending rate decreased slightly, but the hydrogel actuator with a layer thickness ratio of 1:1 (i.e., 1.0 mm for $N_{97}S_3M_3$ and 1.0 mm for $N_{100}M_3$) still reached the maximum bending angle (i.e., 90°) from 44° in 120 s. However, when the thickness ratio increases to 3:1 (i.e., 1.5 mm for $N_{97}S_3M_3$ and 0.5 mm for $N_{100}M_3$), the bilayer hydrogel slightly bent from 16° to about 30° and then remained unchanged. Figure S7b, Supporting Information illustrated the bending rates of $N_{97}S_3M_3$-$N_{100}M_3$ bilayer hydrogels with varying thickness ratios, and they were determined to be 0.53° s^{-1} at thickness ratio of 1:3, 0.34° s^{-1} at thickness ratio of 1:1, and 0.52° s^{-1} at thickness ratio of 3:1, respectively. This phenomenon is likely due to the fact that, as the majority of the bilayer hydrogel was $N_{97}S_3M_3$, whose LCST was higher than the ambient temperature, the bilayer hydrogel layer did not experience a phase transition process in the test. The thermo-responsive behavior of bilayer hydrogels with different $N_{100-y}S_yM_3$ layer (1 mm of $N_{100-y}S_yM_3$ and 1 mm of

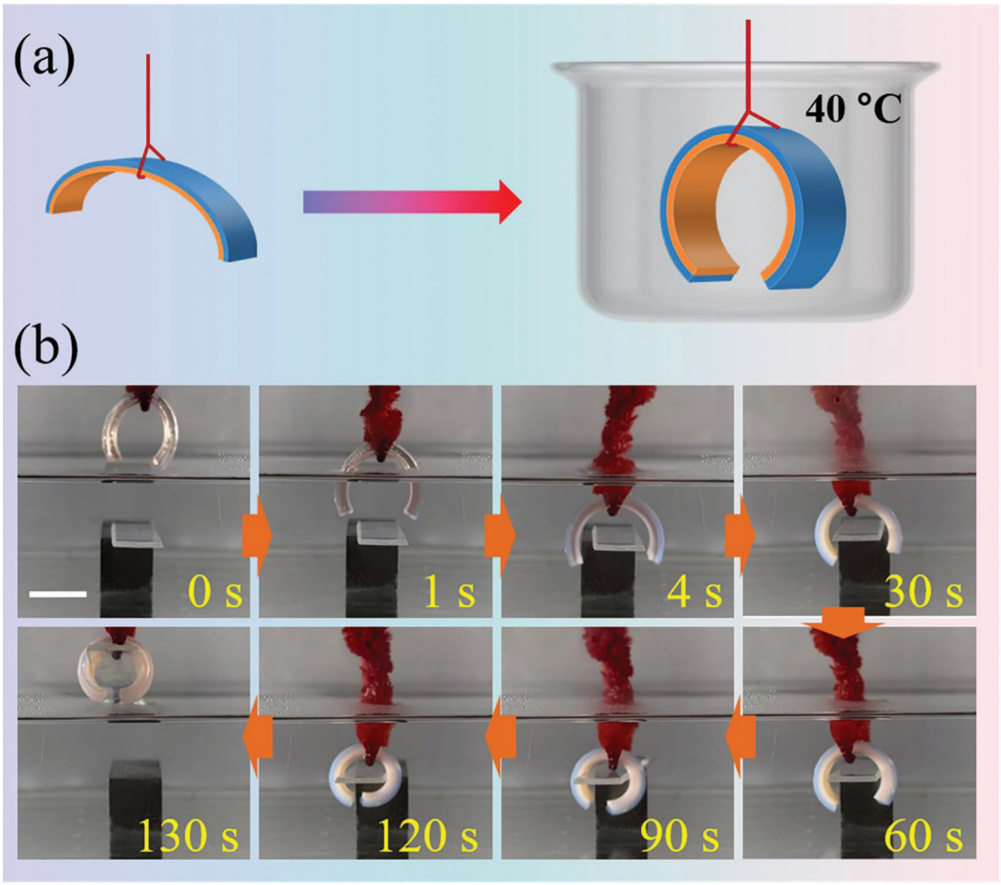

Figure 7. a) Schematic diagram illustrating deformation of a bilayer soft actuator (thickness ratio of $N_{97}S_3M_3$ layer to $N_{100}M_3$ layer is 1:1) at an elevated temperature. b) Snapshots of a bilayer hydrogel gripper capturing an object in water bath at 40 °C. Scale bar is 1 cm.

$N_{100}M_3$ layer) was also investigated (Figure S8, Supporting Information). At 40 °C, the time bent from its initial state to 90° was 60, 120, and 420 s for $N_{99}S_1M_3$-$N_{100}M_3$, $N_{97}S_3M_3$-$N_{100}M_3$, and $N_{95}S_5M_3$-$N_{100}M_3$, respectively. Notably, as the SMA content in the $N_{100-y}S_yM_3$ layer increased, the bending rate of the actuator gradually decreased, from 0.77° s^{-1} of $N_{99}S_1M_3$-$N_{100}M_3$ hydrogel, to 0.34° s^{-1} of $N_{97}S_3M_3$-$N_{100}M_3$ hydrogel, and finally to 0.10° s^{-1} of $N_{95}S_5M_3$-$N_{100}M_3$ hydrogel (Figure S7c, Supporting Information). In summary, it can be seen that the bending speed and bending rate of the bilayer hydrogel could be precisely controlled by external temperature as well as the thickness ratio of the layers.

Using $N_{97}S_3M_3$-$N_{100}M_3$ as a representative example, it showed responsiveness and shape recovery in deionized water when subjected to temperature fluctuations from 40 to 20 °C (Figure S9, Supporting Information). After undergoing a bending-releasing-bending behavior, noticeable reduce in both initial bending angle and bending speed was observed.

3.8. Demonstration of a Bilayer Hydrogel as a Temperature-Controlled Actuator

Shape-variable soft actuators have potential applications in areas such as soft grippers and robotic arms. Thanks to the excellent mechanical properties and distinctive thermo-responsiveness, the hydrogels were assembled into bilayer hydrogel devices. As shown in **Figure** 7a, a bilayer hydrogel with a length of 25 mm and a width of 5 mm was constructed, which could be used as a gripper at an elevated temperature. Figure 7b shows the process of the bilayer hydrogel actuator grasping a plastic plate. When the hydrogel gripper was placed in a water bath at 40 °C, it quickly bent, and grasped the plastic plate in ≈90 s (Movie S2, Supporting Information). In another demonstration, a temperature-responsive hydrogel flower was assembled using two hydrogel petals of the same size, fixed with a pin in the center. The intelligent artificial flower showed a closing process within 150 s when it was placed in a water bath at 40 °C (**Figure** 8 and Movie S3, Supporting Information). In summary, it has been demonstrated that the thermo-responsive microgel-crosslinked hydrogel exhibits a temperature-responsive property, making it suitable for a wide range of applications in fields such as soft robotics and mechanical grasping.

4. Conclusion

In summary, PNIPAM hydrogels with outstanding mechanical properties and rapid thermo-responsive behavior were fabricated by crosslinking with vinyl-functionalized microgels. The obtained hydrogels exhibited excellent toughness. The

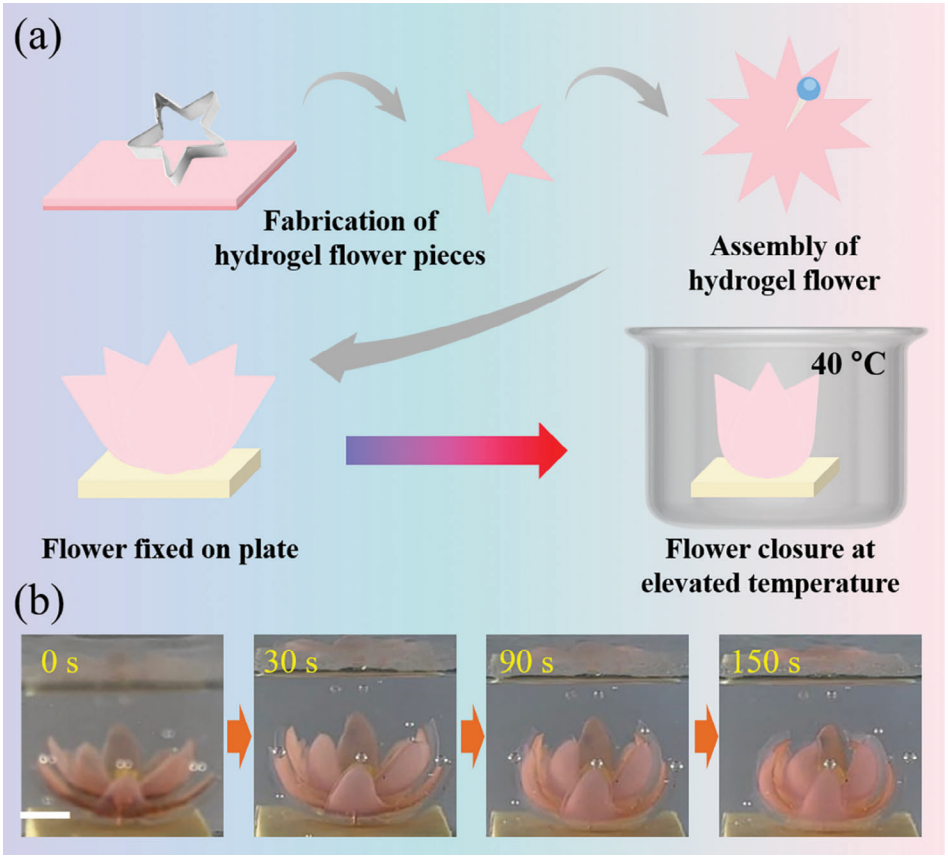

Figure 8. a) Schematic diagram illustrating an artificial flower made from bilayer hydrogel (thickness ratio of $N_{97}S_3M_3$ layer to $N_{100}M_3$ layer is 1:1) deformed at an elevated temperature. b) Closing process of a bilayer hydrogel flower in water bath at 40 °C. Scale bar is 1 cm.

microgel crosslinking points allow for energy dissipation upon compression and stretching of the bulk hydrogels. The LCST of the PNIPAM hydrogels was tuned by varying the content of MGV crosslinkers and ionic units of SMA. Bilayer hydrogel was prepared through a layer-by-layer method, which was sensitive to the changes in temperature and exhibits thermo-responsive bending capabilities. A manipulator was made from the bilayer hydrogel, and it showed good grasping capability. Artificial flowers constructed from the bilayer hydrogel also demonstrated excellent thermo-responsiveness. This study proposed a simple and convenient method for the preparation of hydrogel construction with improved mechanical properties and fast thermo-responsiveness, and it would have great potential applications in actuators.

Supporting Information

Supporting Information is available from the Wiley Online Library or from the author.

Acknowledgements

This work was supported by Youth Innovation Promotion Association CAS (2021296), Key Research and Development Program of Ningbo (2022Z132), Foundation of Director of Ningbo Institute of Materials Technology and Engineering CAS (2021SZKY0301), and Ningbo Public Welfare Science & Technology Major Project (2021S106).

Conflict of Interest

The authors declare no conflict of interest.

Author Contributions

Y.Y. and Y.X. contributed equally to this work. Y.Y.: Methodology, Investigation, Writing – Original Draft, Visualization. Y.X.: Conceptualization, Methodology, Investigation, Writing – Original Draft, Writing – Review & Editing, Visualization, Funding Acquisition. X.W.: Methodology. J.D.: Methodology. R.W.: Investigation. A.L.: Investigation. H.C.: Investigation. R.W.: Conceptualization, Writing – Review & Editing, Funding Acquisition, Supervision.

Data Availability Statement

The data that support the findings of this study are available from the corresponding author upon reasonable request.

Keywords

bilayer hydrogel actuators, mechanical strength, microgel, poly(*N*-isopropylacrylamide), response rate

Received: November 8, 2023
Revised: December 23, 2023
Published online:

[1] X. Wang, N. Jiao, S. Tung, L. Liu, *ACS Appl. Mater. Interfaces* **2019**, *11*, 30290.
[2] X. Zhang, S. Aziz, B. Salahuddin, Z. Zhu, *Matter* **2023**, *6*, 2735.
[3] L. Hu, T. Shu, Y. Wan, C. Fang, F. Gao, M. J. Serpe, *Mol. Syst. Des. Eng.* **2021**, *6*, 108.
[4] Z. Chen, Y. Chen, M. S. Hedenqvist, C. Chen, C. Cai, H. Li, H. Liu, J. Fu, *J. Mater. Chem. B* **2021**, *9*, 2561.
[5] J. Li, Q. Ma, Y. Xu, M. Yang, Q. Wu, F. Wang, P. Sun, *ACS Appl. Mater. Interfaces* **2020**, *12*, 55290.
[6] C. Cui, C. Shao, L. Meng, J. Yang, *ACS Appl. Mater. Interfaces* **2019**, *11*, 39228.
[7] Y. Cheng, C. Huang, D. Yang, K. Ren, J. Wei, *J. Mater. Chem. B* **2018**, *6*, 8170.
[8] Y. Yang, Y. Tan, X. Wang, W. An, S. Xu, W. Liao, Y. Wang, *ACS Appl. Mater. Interfaces* **2018**, *10*, 7688.
[9] M. Filippi, B. Dasen, J. Guerrero, F. Garello, G. Isu, G. Born, M. Ehrbar, I. Martin, A. Scherberich, *Biomaterials* **2019**, *223*, 119468.
[10] S. Long, J. Huang, J. Xiong, C. Liu, F. Chen, J. Shen, Y. Huang, X. Li, *Polymers* **2023**, *15*, 786.
[11] D. Jiao, Q. L. Zhu, C. Y. Li, Q. Zheng, Z. L. Wu, *Acc. Chem. Res.* **2022**, *55*, 1533.
[12] X. Li, Y. Cheng, J. Zhang, Y. Hou, X. Xu, Q. Liu, *J. Mater. Chem. B* **2022**, *10*, 120.
[13] F. Cheng, H. Chen, H. Li, *J. Mater. Chem. B* **2021**, *9*, 1762.
[14] X. Zhang, J. Xiang, Y. Hong, L. Shen, *Macromol. Rapid Commun.* **2022**, *43*, 2200075.
[15] P. Kujawa, F. Segui, S. Shaban, C. Diab, Y. Okada, F. Tanaka, F. M. Winnik, *Macromolecules* **2006**, *39*, 341.
[16] Y. Zhao, X.-J. Ju, L.-P. Zhang, W. Wang, Y. Faraj, L.-B. Zou, R. Xie, Z. Liu, L.-Y. Chu, *New J. Chem.* **2019**, *43*, 9507.
[17] E. Lee, D. Kim, S. Y. Yang, J.-W. Oh, J. Yoon, *Polym. Chem.* **2017**, *8*, 6786.
[18] J. Mao, Q. J. Yu, S. Wang, *Polym. Adv. Technol.* **2021**, *32*, 1752.
[19] C.-L. Zhang, F.-H. Cao, J.-L. Wang, Z.-L. Yu, J. Ge, Y. Lu, Z.-H. Wang, S.-H. Yu, *ACS Appl. Mater. Interfaces* **2017**, *9*, 24857.
[20] L.-W. Xia, R. Xie, X.-J. Ju, W. Wang, Q. Chen, L.-Y. Chu, *Nat. Commun.* **2013**, *4*, 2226.
[21] J. Liao, H. Huang, *Cellulose* **2020**, *27*, 825.
[22] H. Gu, G. Wang, X. Cao, *J. Appl. Polym. Sci.* **2021**, *138*, 51509.
[23] G. Malucelli, J. Dore, D. Sanna, D. Nuvoli, M. Rassu, A. Mariani, V. Alzari, F. Chem, **2018**, *6*, 585.
[24] J. Liu, L. Jiang, S. He, J. Zhang, W. Shao, *Chem. Eng. J.* **2022**, *433*, 133496.
[25] Z. Liu, Y. Faraj, X. Ju, W. Wang, R. Xie, L. Chu, *J. Polym. Sci., Part B: Polym. Phys.* **2018**, *56*, 1306.
[26] A. Ahiabu, M. J. Serpe, *ACS Omega* **2017**, *2*, 1769.
[27] X.-Z. Zhang, X.-D. Xu, S.-X. Cheng, R.-X. Zhuo, *Soft Matter* **2008**, *4*, 385.
[28] J. Fu, *J. Polym. Sci., Part B: Polym. Phys.* **2018**, *56*, 1336.
[29] J. Hu, K. Hiwatashi, T. Kurokawa, S. M. Liang, Z. L. Wu, J. P. Gong, *Macromolecules* **2011**, *44*, 7775.
[30] J. Jang, J. Park, I. Kim, J. Sim, S. Yu, D. Lee, Y. Lee, S. Park, H. Kim, *J. Appl. Polym. Sci.* **2021**, *138*, 49788.
[31] M. Chen, L. Zhou, Y. Guan, Y. Zhang, *Angew. Chem., Int. Ed.* **2013**, *125*, 10145.
[32] J. Xue, W. Bai, H. Duan, J. Nie, B. Du, J. Z. Sun, B. Z. Tang, *Macromolecules* **2018**, *51*, 5762.
[33] R. Das Mahapatra, K. B. C. Imani, J. Yoon, *ACS Appl. Mater. Interfaces* **2020**, *12*, 40786.
[34] H. Wang, P. Li, K. Xu, Y. Tan, C. Lu, Y. Li, X. Liang, P. Wang, *Colloid Polym. Sci.* **2016**, *294*, 367.
[35] K. Murakami, A. Imai, A. Nakamura, *Colloids Surf. A* **2023**, *674*, 131944.
[36] L.-W. Xia, X.-J. Ju, J.-J. Liu, R. Xie, L.-Y. Chu, *J. Colloid Interface Sci.* **2010**, *349*, 106.
[37] G. Hoti, F. Caldera, C. Cecone, A. Rubin Pedrazzo, A. Anceschi, S. L. Appleton, Y. Khazaei Monfared, F. Trotta, *Materials* **2021**, *14*, 478.
[38] M. Kessler, T. Yuan, J. M. Kolinski, E. Amstad, *Macromol. Rapid Commun.* **2023**, *44*, 2200864.
[39] C. Jin, W. Song, T. Liu, J. Xin, W. C. Hiscox, J. Zhang, G. Liu, Z. Kong, *ACS Sustainable Chem. Eng.* **2018**, *6*, 1763.
[40] S. Ida, S. Toda, M. Oyama, H. Takeshita, S. Kanaoka, *Macromol. Rapid Commun.* **2021**, *42*, 2000558.
[41] J. Hu, T. Kurokawa, T. Nakajima, T. L. Sun, T. Suekama, Z. L. Wu, S. M. Liang, J. P. Gong, *Macromolecules* **2012**, *45*, 9445.
[42] B. Strachota, A. Strachota, G. Gąsior, M. Šlouf, *J. Polym. Res.* **2021**, *28*, 211.
[43] B. Strachota, K. Oleksyuk, A. Strachota, M. Šlouf, *Eur. Polym. J.* **2019**, *120*, 109213.
[44] D. Sarmah, N. Karak, *J. Appl. Polym. Sci.* **2020**, *137*, 48495.
[45] B. Strachota, A. Strachota, S. Horodecka, M. Šlouf, J. Dybal, *J. Mater. Res. Technol.* **2021**, *15*, 6079.
[46] B. Strachota, A. Strachota, M. Šlouf, J. Brus, V. Cimrová, *Soft Matter* **2019**, *15*, 752.